UDC 621.313 https://doi.org/10.20998/2074-272X.2024.3.02

M.M. Zablodskiy, R.M. Chuenko, S.I. Kovalchuk, H.V. Kruhliak, O.I. Kovalchuk

Internal capacitive compensation of the reactive power of the screw electromechanical converter

Introduction. *A special category among induction machines with a massive rotor is occupied by the class of multifunctional electromechanical energy converters, which are integrated with the links of technological processes* ***Problem.*** *The exchange of reactive energy between the source and the electromechanical converter during periods of operation with a low load leads to a significant decrease in its efficiency and power factor. With the use of non-linear loads and taking into account possible resonance, it has become more difficult to improve the power factor by installing capacitor banks.* ***Goal.*** *Increasing the energy indicators of the electromechanical converter by spatial displacement of the main and additional stator windings and internal capacitive compensation.* ***Methodology.*** *Comparative analysis of connection schemes and spatial arrangement of stator windings when using internal capacitive compensation. Modeling and experimental studies of electromagnetic and electromechanical characteristics of a screw electromechanical converter.* ***Results****. The distribution of electromagnetic quantities was established and the choice of the angle of spatial displacement of the main and additional windings of the stator phases of the modified converter, which ensure an increase in the value of the electromagnetic torque and power factor, was justified. The results of experimental studies of the screw electromechanical converter are presented.* ***Originality.*** *For the first time, a method of internal capacitive compensation of reactive power is proposed for multifunctional electromechanical converters of technological purpose.* ***Practical value.*** *The use of the proposed method of spatial displacement of the main and additional stator windings and internal capacitive compensation will ensure an increase in the energy performance of the screw electromechanical converter.* References 23, tables 3, figures 15.
Key words: **Maxwell's equation, multifunctional electromechanical converter, stator winding, finite element method, capacitor capacity.**

Вступ*. Особливу категорію серед асинхронних машин з масивним ротором займає клас поліфункціональних електромеханічних перетворювачів енергії, які інтегровані з ланками технологічних процесів.* ***Проблема****. Обмін реактивною енергією між джерелом і електромеханічним перетворювачем в періоди роботи з низьким навантаженням приводить до суттєвого зниження його ефективності і коефіцієнта потужності. З використанням нелінійних навантажень і урахуванням можливого резонансу покращити коефіцієнт потужності встановленням батарей конденсаторів стало складніше.* ***Мета****. Підвищення енергетичних показників шнекового електромеханічного перетворювача шляхом внутрішньої ємнісної компенсації реактивної потужності.* ***Методологія****. Порівняльний аналіз схем з'єднання і просторового розташування обмоток статора при застосуванні внутрішньої ємнісної компенсації. Моделювання та експериментальні дослідження електромагнітних і електромеханічних характеристик шнекового електромеханічного перетворювача.* ***Результати****. Встановлено розподіл електромагнітних величин і обґрунтовано вибір кута просторового зміщення основної і додаткової обмоток фаз статора модифікованого перетворювача, які забезпечують збільшення електромагнітного моменту та коефіцієнта потужності. Наведено результати експериментальних досліджень шнекового електромеханічного перетворювача.* ***Оригінальність****. Вперше для поліфункціональних електромеханічних перетворювачів технологічного призначення запропоновано метод внутрішньої ємнісної компенсації реактивної потужності.* ***Практичне значення****. Використання запропонованого методу просторового зміщення основної і додаткової обмоток статора та внутрішньої ємнісної компенсації забезпечить підвищення енергетичних показників шнекового електромеханічного перетворювача.* Бібл. 23, табл. 3, рис. 15.
Ключові слова: **рівняння Максвелла, поліфункціональний електромеханічний перетворювач, обмотка статора, метод скінченних елементів, ємність конденсатора.**

Introduction. The dominant part of electric motors used in industry are three-phase induction motors (IMs) with a short-circuited rotor. However, in the most widely used IMs with power of up to 11 kW, the efficiency and the power factor cosφ are very low and amount to 0,7-0,9. The exchange of reactive energy between the source and the consumer leads to the appearance in the system of an additional, unproductive reactive current in addition to the active current, overloading of all elements of the electrical system, including the source, the consumer and the power transmission line. In addition, in periods of operation with a low load, it is necessary to take into account the factor of a significant decrease in the efficiency and power factor of the motors. Thus, variable frequency drives for IMs require mechanisms for at least internal buffering of energy for reactive power at the network frequency to correct the power factor and organize effective control [1, 2]. The traditional approach to power factor correction in industrial applications involves installing capacitor banks with microcontrollers for switching synchronous capacitors [3]. The use of parallel capacitor compensation during switching on and start-up is effective in reducing the transient current in large induction motors [4]. But with the widespread use of non-linear loads such as variable speed drives, improving power factor has become more difficult. The resonance problem arises from power system inductance and compensation capacitors, which increases harmonic distortion. A new method of damping harmonic resonances in the power supply system is proposed in [5]. The main feature of this technique is that the active static compensation circuit can simultaneously work as a harmonics injector, a power factor corrector, and a resonance eliminator. But the proposed model is developed only for a single-phase system and should be extended for a three-phase system with different linear and non-linear loads.

The use of automatic switching of the connection of the stator winding in motors with a variable load is common. In [6], the concept of a multi-flow motor with various possible connections of the windings, which allow adjusting the magnetizing flux at six different levels, is proposed. At the same time, the efficiency and power factor of motors can be significantly improved at low load. Compared to the savings potential for the corresponding loads, the additional cost of such a motor is not high, but the cost of automatic switching equipment (control device and contactors) can be significant.

In [7], multi-cascaded induction motors, which are mechanically connected in the form of a cascade with the same power, are considered. In addition, to compare the results, a single induction motor (SIM) is considered, the power of which is the sum of the powers of all multi-cascade induction motors (MCIM). The effect of balance voltage and unbalanced frequency on the highest and stable torque, power factor, active and reactive input power, and losses was studied. The results show the highest torque of MCIM compared to SIM. Also, copper losses are reduced when MCIM is used instead of SIM. As a result, the energy conversion procedure is significantly improved.

Problem definition. A special category of induction machines consists of electric motors with a massive (solid) rotor made of ferromagnetic steel, which, thanks to their rigid construction and integrity, can operate at the highest required rotation speeds. Another useful feature of these machines is their ability to operate in aggressive environments and environments with high humidity. The disadvantage of this design is a relatively low power factor compared to machines with a short-circuited cage or permanent magnets [8]. At the same time, today a promising class of multifunctional electromechanical energy converters is being formed, in which constructive and functional integration with links of technological processes is provided. At the same time, all types of dissipative energy component of electromechanical converters are used in the technological process, in particular, for the processing of raw materials. The external massive rotor, for example, of the screw electromechanical converter (SEMC), combined with the executive body – the screw, is in direct contact with the loading and cooling medium and is able to form multiphysics processes of processing raw materials [9]. To increase the power factor of the SEMC, a means of reactive power compensation is required. This article proposes a method that overcomes most of the drawbacks noted above.

The goal of the work is to increase the energy performance of the screw electromechanical converter by means of internal capacitive compensation of reactive power.

Analysis of recent research and publications. In the practice of researching the parameters and characteristics of electromechanical converters, the methods of numerical field calculations, substitution circuits, are widely used, which significantly increases the accuracy of the results of the analysis of the reconfiguration of windings and magnetic systems.

In [10], a method for calculating active and reactive parameters of windings, mechanical characteristics of an induction motor with a short-circuited rotor based on a numerical field approach is proposed, which does not require conditional correction coefficients and reference graphic functions. An increase in magnetic conductivities was revealed due to a more natural structure of the lines of force of the magnetic field in the upper parts of the slots, while the classical technique is a priori based on an overly simplified structure of the lines of force.

The work [11] is aimed at reviewing and analyzing various methods that are used to determine the parameters of the substitution circuit and transient characteristics of a three-phase induction motor under different conditions. In [12], an accurate procedure for calculating the losses in the iron core is proposed, which is used in the model of the substitution circuit of an induction machine to improve the calculations of the machine's performance. An important factor in the calculation procedure is taking into account the surface effect and magnetic saturation, as well as the effect of the change in the temperature of the iron core on the losses in it.

The authors of the work [13] investigated the influence of the angular shift in the arrangement of windings for a double three-phase stator winding of an induction motor with a short-circuited rotor with an emphasis on the relationships of phase flow, speed characteristics and torque characteristics.

In recent years, a large amount of research has focused on methods of increasing the energy efficiency of external rotor induction motors with a split phase winding operating with high slip. In [14], an analytical model based on a magnetic equivalent circuit is proposed to evaluate the performance of induction motors with a short-circuited external rotor, which are widely used in ceiling fans, pumps, and wheel drives. In addition, copper losses in the windings and iron losses in the core are calculated using the proposed model. The results of the presented model are compared with the results of transient finite element analysis, and the experimental measurements closely match the results confirming the success of the proposed model in terms of accuracy. Issues of inaccuracy in the equivalent circuit method for applications in low power motors for external rotor geometry are discussed in [15] with experimental verification using different equivalent circuit approaches.

The work [16] presents a new six-phase induction motor with an external rotor, equipped with pseudo-concentrated windings. Several aspects of the proposed motor design, such as the design algorithm and analytical modeling based on the modified winding function considering the skew effect, are investigated. An appropriate optimization task is also defined for maximizing the power factor and efficiency and minimizing output torque ripples.

Three-phase induction motors of small and medium power are most dominant in the industrial sector, providing a wide range of constant and variable speeds and loads where dynamic response requirements are not critical, such as pumps, fans and compressors. However, they are still burdened by low power factor at partial loads, which can only be mitigated by adding power factor correction capacitors. In [17], in contrast to variable-speed drives, which have torque or speed control and use pulse-width modulation strategies [5-7], it is proposed to overcome the typical disadvantages of conventional induction motors, mainly low efficiency and power factor, by using less expensive partial power converter. According to the approach [17], a special induction machine is used, which includes a main winding connected to the network and an auxiliary three-phase winding with a smaller number of turns, located in the same slots of the stator as the main one. The auxiliary winding is powered by a voltage inverter with a floating DC bus capacitor. A strategy is implemented to effectively control the power factor, mitigate the harmful effects associated with distorted mains voltage and mechanical torque vibrations, and reduce the large inrush current caused by the induction motor during the starting period. First, the proposed technique is presented theoretically then the feasibility assessment is performed by modeling.

For high-speed induction machines with a solid rotor, which have high eddy current losses, the use of a two-layer asymmetric winding with a short step and collecting coils is known. However, the asymmetrical winding also introduces some current imbalance due to the three-phase asymmetrical stator inductance. Current imbalance can have harmful effects on both the machine and the power supply, such as torque ripple, unbalanced magnetic attraction, and thermal load on the power supply network and power electronics. To mitigate the current imbalance, the work [18] proposes an improvement of the method, which consists in slightly increasing the height of the stator slot and placing the sides of the coil above or below within the slot height for different phases. Based on the 2D finite element method, the stator slot height is optimized in terms of current unbalance mitigation. Using the result of the optimization, they proceed to additional adjustment of the position of the coil for a specific phase. Unlike conventional power electronics current imbalance mitigation methods, the proposed method suppresses current imbalance solely by adjusting the machine design, which avoids additional investment for power electronics devices.

Therefore, the methods of reducing eddy current losses for machines with a solid rotor considered above are associated with the occurrence of current imbalance and additional complications of power electronics devices. But for SEMCs, taking into account the scope of their functional tasks [9, 19], the problem of reducing eddy current losses in the rotor is not critical, with the exception of effective control of the power factor.

Comparative analysis of the connection schemes and spatial arrangement of the stator windings of the basic and modified versions of SEMC. The SEMC is presented in Fig. 1, which shows its electromagnetic system and calculation scheme for modeling.

As stators of the basic version, the moving part of the MTF-011-6 crane motor with nominal power P_n = 1,4 kW, phase connection scheme – star, number of poles $2p$ = 6, winding type – single-layer concentric was used.

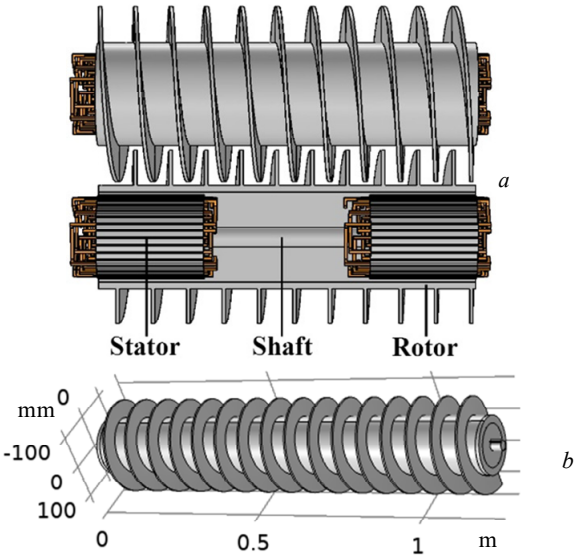

Fig. 1. SEMC: electromagnetic system (*a*); calculation scheme (*b*)

To increase the rotational electromagnetic torque of the modified device, it is proposed to use internal capacitive compensation of reactive power [20]. In the stator of the basic SEMC, a single-layer concentric winding with a full step (Fig. 2,*a*) is used, which has one parallel branch (a = 1). Here, the number of coils in the coil group is 2. In the modified SEMC, a winding with two parallel turns a = 2 is used, in this case, the number of coils in the coil group is reduced to one, and the number of coil groups is doubled (Fig. 2,*b*).

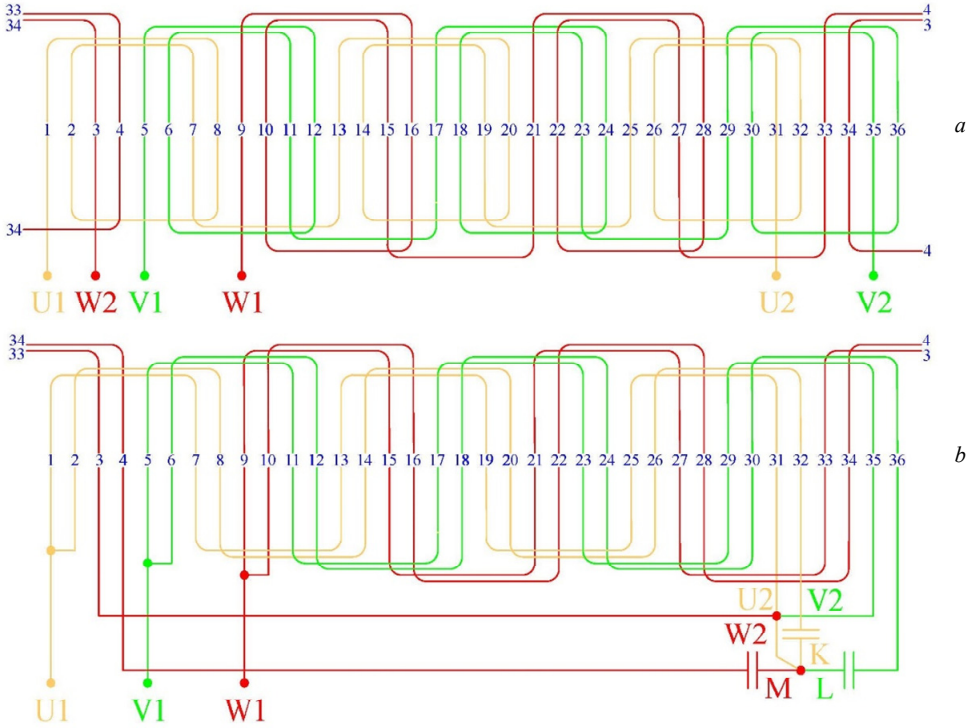

Fig. 2. Expanded electrical diagrams of the stator windings of the basic (*a*) and modified (*b*) SEMC

One of the parallel branches forms the so-called main or working winding, which is connected to the power supply network. Another parallel branch, displaced in the slots of the core by 30° relative to the main

winding, forms an additional winding, which is switched on according to the circuit of a rotary autotransformer on electrical capacity (Fig. 3,*a*).

The use of internal capacitive compensation of the modified SEMC for a wide range of changes in the angle of spatial displacement of the main and additional windings and compensating capacitors allows changing the value and phase of currents, magnetomotive forces and other electrical quantities. As a result, there is an opportunity to increase the energy efficiency and torque of the modified SEMC. Unlike the basic SEMC, where the current of the single stator winding has an active-inductive character both in the starting and operating modes of operation, the stator winding of the modified SEMC has two working turns. The current of the main winding I_1 retains an active-inductive character, and the current of the additional winding I_Δ with a capacitor connected in series acquires a capacitive-active character (Fig. 3,*b*).

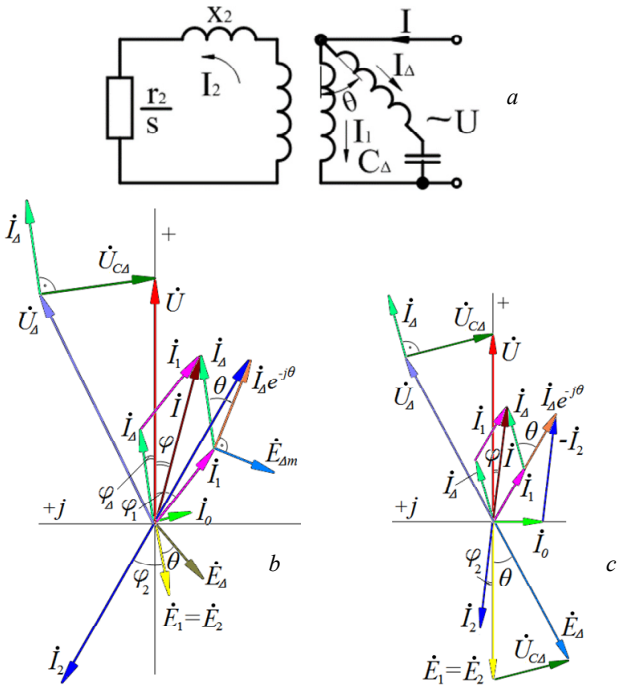

Fig. 3. Schematic electrical diagram of the phase (*a*) and vector diagram during start-up (*b*) and at nominal load (*c*) of the modified SEMC

The current I_Δ depends not only on the supply voltage and machine parameters, but also on the capacity of the capacitor C_Δ. The current $\dot{I}_\Delta e^{-j\theta}$, as reduced to the axis of the main phase winding of the stator, participates in the creation of the magnetizing current of the device $\dot{I}_0 = \dot{I}_1 + \dot{I}_\Delta e^{-j\theta} + \dot{I}_2$ and creates an additional EMF $\dot{E}_{\Delta m} = -jx_m \dot{I}_\Delta e^{-j\theta}$. The EMF $\dot{E}_{\Delta m}$ induced by the spatially shifted current $\dot{I}_\Delta$ of the additional winding increases the main EMF of the stator and rotor. An increase in the EMF of the rotor with its constant active and inductive resistances leads to an increase in the starting current of the rotor, and, therefore, the starting torque of the modified SEMC. Under the influence of the increased starting torque, the acceleration process of the device is accelerated and it reaches a tougher mechanical characteristic in the operating mode compared to the basic SEMC. The vector diagram of the modified SEMC under the nominal load is shown in Fig. 3,*c*.

The angle of spatial displacement of the main and additional windings of the stator phases of the modified SEMC of 30° was chosen in view of the fact that precisely at this angle, an increase of 20-30 % of the starting torque is provided at a constant starting current compared to the basic device. The technological simplicity of performing the stator windings of the modified SEMC by dividing the 60° phase zone of the basic device winding into two equal parts is also taken into account [20].

Initial conditions for modeling electromagnetic and electromechanical characteristics of SEMC. Modeling was carried out for SEMC with the following parameters: stator core length L_s = 90 mm; the length of the corresponding section of the common external rotor L_r = 300 mm; current frequency f_0 = 50 Hz; angular speed $\omega_0 = 2\pi f_0$, rad/s; volume density of rotor steel ρ_{st} = 7850 kg/m^3; amplitude value of the current $I_0 = 13\sqrt{2}$ A; t is the time parameter.

Basic device variables: phase U current $I_U = I_0 \cdot \sin(\omega_0 \cdot t)$ A; phase W current $I_W = I_0 \cdot \sin(\omega_0 \cdot t + 120°)$ A; phase V current $I_V = I_0 \cdot \sin(\omega_0 \cdot t - 120°)$ A.

Variables of the modified device: phase U current $I_U = I_0 \cdot \sin(\omega_0 \cdot t)$ A; phase W current $I_W = I_0 \cdot \sin(\omega_0 \cdot t + 120°)$ A; phase V current $I_V = I_0 \cdot \sin(\omega_0 \cdot t - 120°)$ A; phase K current $I_K = I_0 \cdot \sin(\omega_0 \cdot t + 30°)$ A; phase M current $I_M = I_0 \cdot \sin(\omega_0 \cdot t + 150°)$ A; phase L current $I_L = I_0 \cdot \sin(\omega_0 \cdot t - 90°)$ A.

The topology of the stator windings of the basic and modified versions of SEMC is shown in Fig. 4.

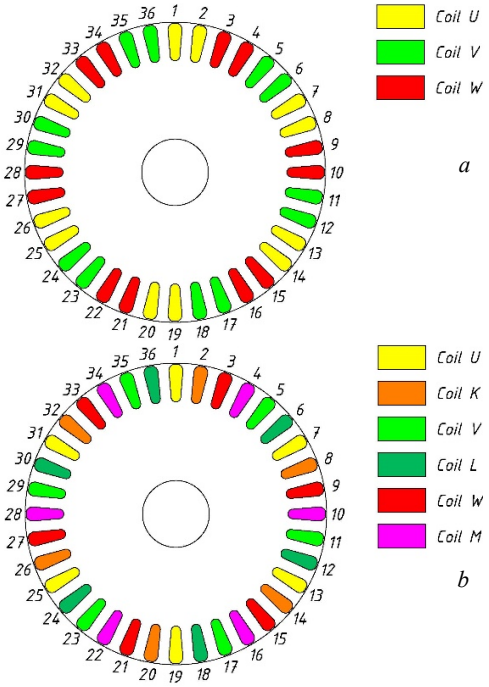

Fig. 4. Topology of SEMC stator windings: basic version (*a*); modified version (*b*)

The characteristics of the modified device both in the starting and operating modes depend on the capacity of the capacitor connected in series with the additional winding. Since the currents of the main and additional windings, the phase of the current of the additional winding, as well as the losses in the motor change in this

case, it is advisable to choose the capacity of the capacitor in the circuit of the additional winding, which provides the same currents in the main and additional windings of the stator phases of the device. To ensure this mode of operation of the modified device, the capacity of the capacitor is 25 μF per 1 kW of rated power.

The simulation was performed in the Comsol Multiphysics software environment [21] according to the calculation scheme (Fig. 1,*b*). Considering the identity of the electromagnetic, electromechanical, thermal and vibrational processes that occur on the «stator-corresponding section of the common rotor» modules of the SEMC electromagnetic system, the simulation was carried out for one of them. If there are differences in parameters or geometric dimensions, the simulation is carried out separately for each stator. The numerical analysis of the electromagnetic field is carried out using a mathematical model of a twin-screw electromechanical hydrolyzer [22]:

$$\nabla\times\boldsymbol{H} = \boldsymbol{J}, \quad (1)$$

where $\boldsymbol{H}$ is the magnetic field strength vector, A/m; $\boldsymbol{J}$ is the current density vector, A/m^2;

$$\boldsymbol{B} = \nabla\times\boldsymbol{A}, \quad (2)$$

where $\boldsymbol{B}$ is the magnetic flux density vector, T; $\boldsymbol{A}$ is the magnetic vector potential, Wb/m;

$$\boldsymbol{E} = -\partial A / \partial t, \quad (3)$$

where $\boldsymbol{E}$ is the electric field strength vector, V/m;

$$\boldsymbol{J} = \sigma\boldsymbol{E}, \quad (4)$$

where σ is the specific electrical conductance, S/m.

The formulation of the scalar potential is performed according to the equation:

$$\nabla\cdot\boldsymbol{B} = 0. \quad (5)$$

At the external boundary with a magnetic scalar potential, the normal component of the magnetic flux density equals zero:

$$n\cdot\boldsymbol{B} = 0. \quad (6)$$

The magnetization of the ferromagnetic rotor is given as a *B-H* curve and is determined from the equation:

$$B = f\left(\left|H\right|\right)\frac{H}{\left|H\right|}. \quad (7)$$

Multi-turn stator windings are used as a current source in the model (Fig. 2, 3). The windings provide the current density in the direction of the conductors J_e according to the equation:

$$J_e = \frac{N\cdot I_{coil}}{A}\cdot e_{coil}, \quad (8)$$

where N is the number of turns in the winding; A is the general section, area of the winding domain, m^2; I_{coil} is the current, A; e_{coil} is the vector variable for visualizing the direction of turns in the winding.

Modeling of thermal parameters was performed by combining the physics of magnetic fields, heat transfer in solids, and electromagnetic heating in the frequency-transition domain of research. The mathematical model of heat transfer is given in the most general form, the initial temperature is 293 K. Heat exchange according to Fourier law in a differential form containing a heat source is described by the following equation [23]:

$$d_z\rho C_p\frac{\partial T}{\partial t} + d_z\rho C_p\boldsymbol{u}\cdot\nabla T + \nabla\cdot q = d_zQ + q_0 + d_zQ_{ted}, \quad (9)$$

where d_z is the thickness of the domain in the non-planar direction, m; ρ is the density, kg/m^3; C_p is the specific heat capacity at constant pressure, J/(kg·K); T is the temperature, K; t is the time, s; $\boldsymbol{u}$ is the velocity vector, m/s; q is the heat flow, W/m^2; Q is the heat source, W/m^3; q_0 is the external heat flow, W/m^2; Q_{ted} is the thermoelastic damping, W/m^3;

$$q = -d_zk\nabla T, \quad (10)$$

where k is the thermal conductivity, W/(m·K).

Thermal insulation is applied to the external boundaries of the model [23]:

$$-n\cdot q = 0, \quad (11)$$

where n is the refractive index.

The heat flow from the surfaces is defined as [23]:

$$-n\cdot q = d_zq_0, \quad (12)$$

$$q_0 = h\cdot(T_{ext} - T) \quad (13)$$

where h is the heat transfer coefficient, W/(m^2·K); T_{ext} is the ambient temperature, K.

Radiation from the surface of the model to the environment is determined from the equation [23]:

$$-n\cdot q = d_z\varepsilon\sigma\cdot(T^4{}_{amb} - T^4), \quad (14)$$

where ε is the emissivity of the surface; σ is the Stefan-Boltzmann constant, W/(m^2·K^4); T_{amb} is the temperature of the environment, K.

Electromagnetic heating is determined from equations [23]:

$$\rho C_p\frac{\partial T}{\partial t} + \rho C_p\boldsymbol{u}\cdot\nabla T = \nabla\cdot\left(k\nabla T\right) + Q_e, \quad (15)$$

where Q_e is the electromagnetic heat source, W/m^3:

$$Q_e = Q_{rh} + Q_{mi}, \quad (16)$$

where Q_{rh} are the resistive losses, W/m^3; Q_{mi} are the magnetic losses, W/m^3:

$$Q_{rh} = 0{,}5\cdot\mathrm{Re}(\boldsymbol{J}\cdot\boldsymbol{E}^*); \quad (17)$$

$$Q_{mi} = 0{,}5\cdot\mathrm{Re}(j\omega\boldsymbol{B}\cdot\boldsymbol{H}^*); \quad (18)$$

where $\boldsymbol{E}^*$ is the electric field strength vector at a given frequency at a certain moment in time, V/m; $\boldsymbol{H}^*$ is the magnetic field strength vector at a given frequency at a certain moment in time, A/m.

Simulation results and discussion. The main part of the characteristics based on the results of the simulation of the basic and modified SEMC is presented in the plane of its cross section. Figure 5 shows the distribution of the *z*-component of the current density. A significant difference in the current density distributions is noted for the slot zones of the stator. For the modified version of SEMC, the number of slots with near-zero current density is half as much as compared to the basic version. In the rotor of the modified version of the SEMC, at the depth of penetration of the electromagnetic wave, 6 sections (by the number of poles) are observed with current density values that are 15 % higher than the current density in the corresponding sections of the basic version of the SEMC.

Figure 6 shows the distribution of the volume density of electrical energy. A comparison of the images indicates that the volumetric electrical energy density of the stator of the modified SEMC is on average 19 % higher than the electrical energy density of the stator of the basic SEMC. Since the concept of «energy» according to physical principles is equivalent to the concept of «work», we are talking about the concentration and potential of active energy in the stator.

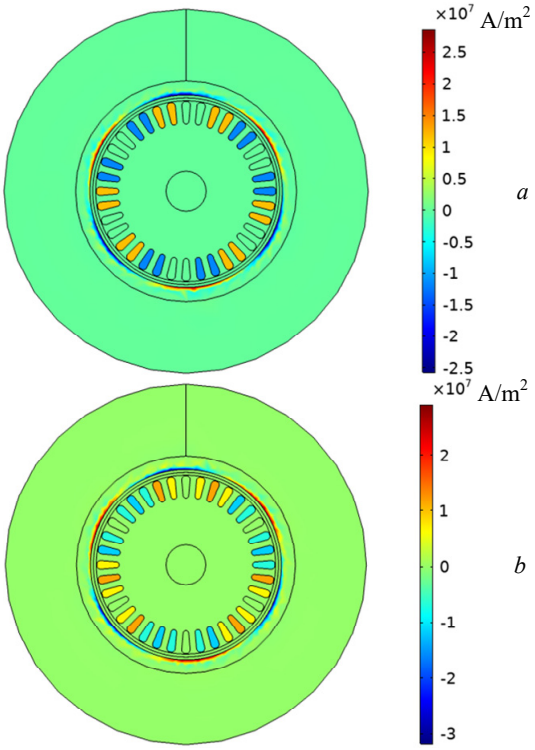

Fig. 5. Current density (*z*-component) of the basic (*a*) and modified (*b*) SEMC

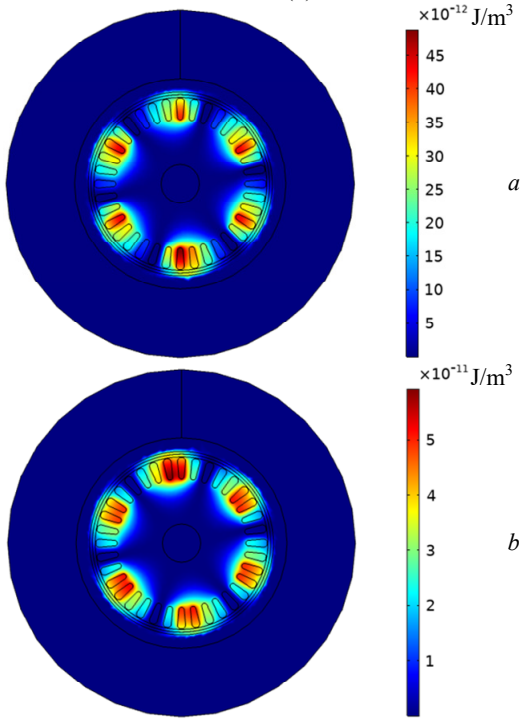

Fig. 6. Volume electrical energy density of the basic (*a*) and modified (*b*) SEMC

Figure 7 shows the time dependence of the electromagnetic torque of the two studied options. For the modified SEMC (Fig. 7,*b*), a significant (1,5 times) increase in value and a decrease in extreme pulsations of the electromagnetic torque were obtained.

Figures 8, 9 present the time dependence and phase angle of the currents of one SEMC module. In the modified SEMC, thanks to the use of internal capacitive compensation, it is possible to change the value and phase of the current of the additional stator winding.

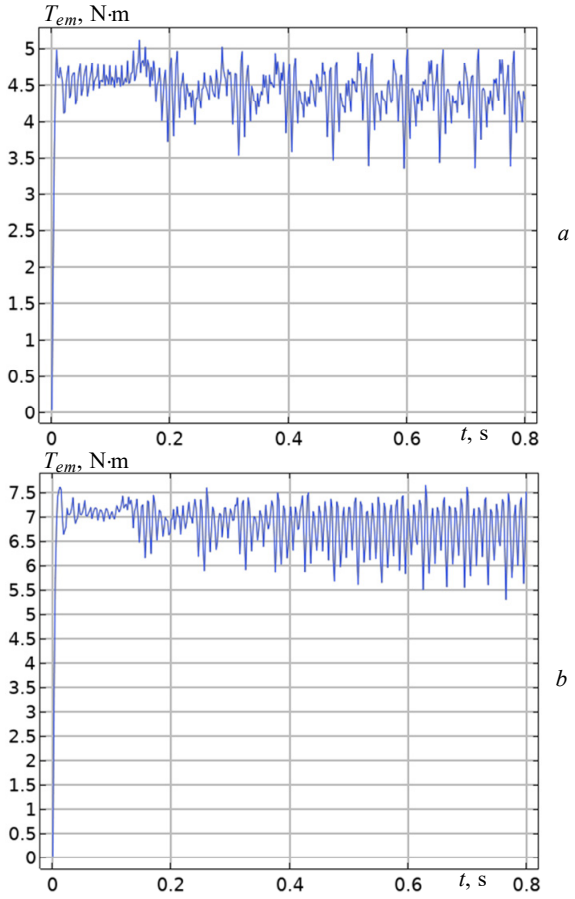

Fig. 7. Electromagnetic torque of the basic (*a*) and modified (*b*) SEMC

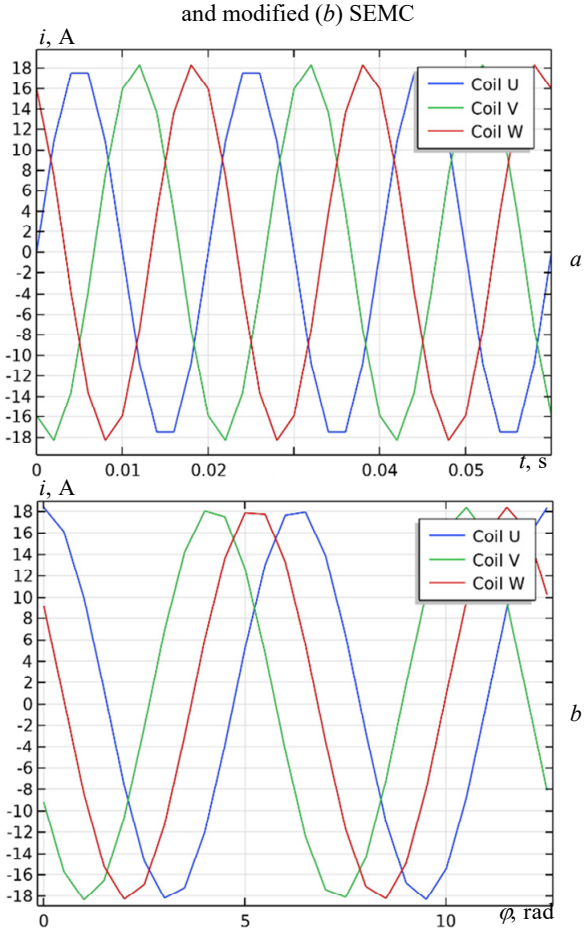

Fig. 8. Time dependence (*a*) and phase angle (*b*) of the currents of one module of the basic SEMC

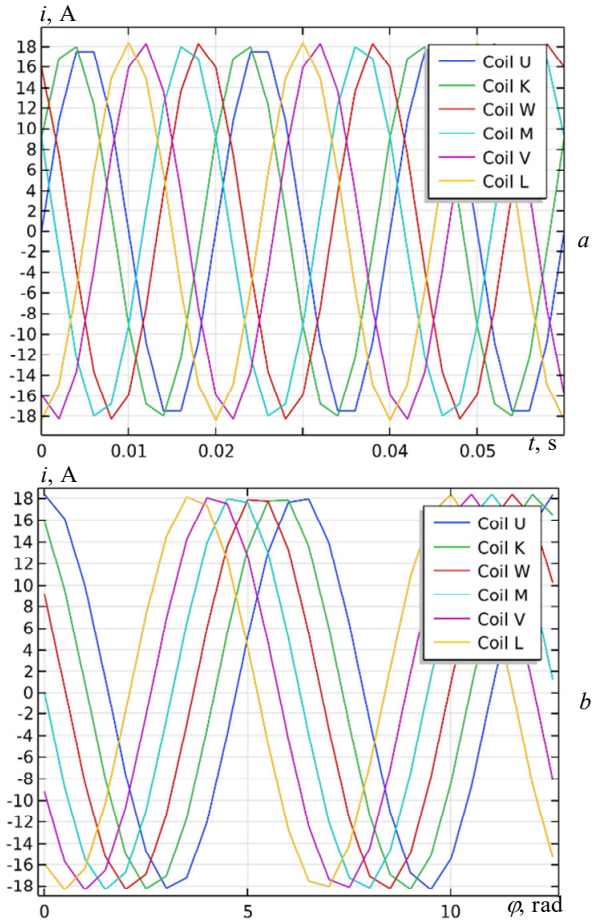

Fig. 9. Time dependence (*a*) and phase angle (*b*) of the currents of one module of the modified SEMC

To increase the torque of the modified SEMC, it is necessary to shift the phase of the current of the additional winding relative to the current of the main winding by 30°. Since in the modified SEMC the main and additional windings are shifted one relative another in space, this leads to an increase in the area of action of the eddy currents created in the rotor. In particular, the angle of the sector occupied by the maximum currents is 2,3 rad for the basic and 2,8 rad for the modified SEMC, respectively. Currents (Fig. 8,*b*) form the resultant magnetomotive force around the circumference of the air gap, the result of which is the creation of eddy currents in the rotor massive. The corresponding zone of action of the generated eddy currents in the rotor massive (Fig. 5) occupies the area opposite 5,5 tooth divisions of the stator for the basic and 6 tooth divisions for the modified SEMC. Therefore, the modified SEMC exceeds the basic SEMC version in terms of current density values and the width of their action zone. As a result of the influence of the phase shift, the SEMC demonstrates the best performance, the best time to establish speed and torque at start-up and load (Fig. 7), which is also observed in induction machines when considering the configuration of a double 3-phase winding [13, 22].

Figure 10 shows the distribution of the magnetic flux density, *X*-*Y* components of the basic and modified SEMC. A significant difference in the distribution of the magnetic flux density for the *X*-*Y* components for the basic and modified SEMC is noted. If for the basic variant, practically the same values of the magnetic flux density for the *X*-*Y* components are observed, for example, opposite the middle of the poles within their instantaneous location, then for the variant of the modified SEMC, the difference in the values of the magnetic flux density along the *X*-*Y* components is quite significant. In addition, a greater degree of branching of the magnetic flux in the stator yoke to the side of the hollow shaft is noted for the version of the modified SEMC.

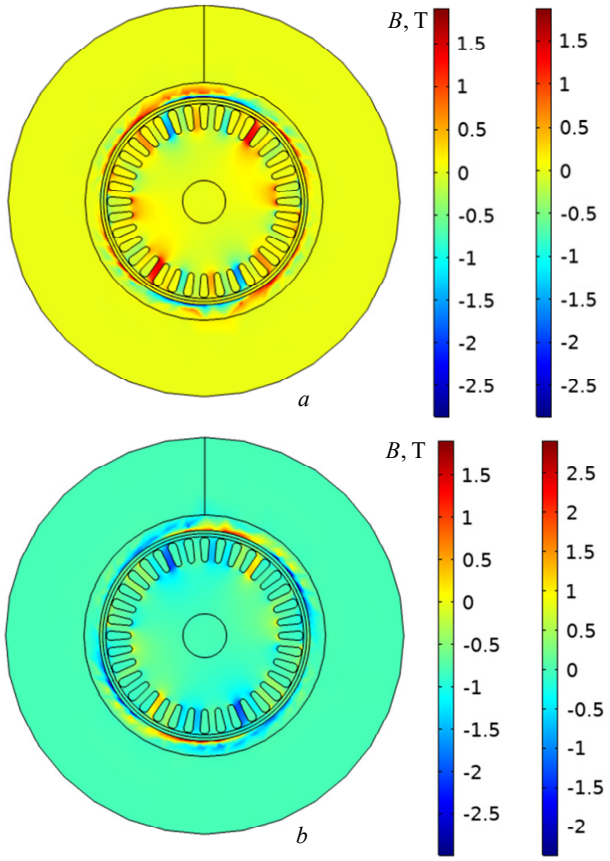

Fig. 10. Magnetic flux density (left legend – *X*-component, right legend – *Y*-component) of the basic (*a*) and modified (*b*) SEMC

This means the presence of a smaller magnetic resistance in the path of the magnetic flux for the variant of the modified SEMC and, accordingly, a smaller reactive power. At the same time, reactive power characterizes the conditions of transmission of active power at each moment of time, and based on Fig. 6, the volume density of the active energy of the stator of the modified SEMC exceeds the density of the active energy of the stator of the basic SEMC, which indirectly indicates a higher value of the power factor of the modified SEMC. This provision is also confirmed by a comparison of the magnetization distribution of the basic and modified SEMCs (Fig. 11).

With the same magnetization in the rotor massive ($2{,}5 \cdot 10^6$ A/m), there is an excess of 23 % of the magnetization of the stator magnetic core in the middle of the poles within the limits of their instantaneous location for the basic ($1{,}5 \cdot 10^6$ A/m) in comparison with the modified SEMC ($1{,}0 \cdot 10^6$ A/m).

Table 1 presents the results of modeling the energy characteristics of the basic and modified SEMCs.

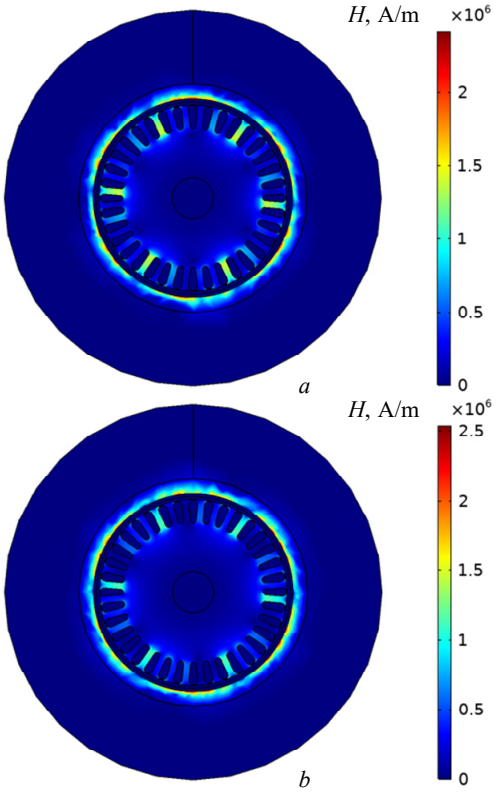

Fig. 11. Magnetization of the basic (*a*) and modified (*b*) SEMC

Table 1

The results of the calculation of the characteristics of the basic and modified SEMC

Indicator	Basic SEMC	Modified SEMC	Difference
Power consumption, W	1080,70	1293,56	212,86
Useful mechanical power, W	103,62	148,60	44,98
Losses in steel, W	484,28	652,13	167,85
Losses in copper, W	492,80	492,80	0
Rotation speed, rpm	180	200	20
Electromagnetic torque, N·m	5,5	7,1	1,6
Efficiency in terms of mechanical power, %	9,58	11,44	1,86
Power factor	0,59	0,71	0,12

The modified SEMC consumes 212,86 W (19,7 %) more active power from the power supply network compared to the basic SEMC. At the same time, the useful active mechanical power increases by 44,98 W (43,4 %) and losses in the steel of the modified SEMC increase by 167,85 W (34,7 %). The copper losses of the modified SEMC do not change compared to the basic device. The modified SEMC creates a 1,6 N·m (29 %) greater electromagnetic torque, as a result of which its rotation frequency increases by 20 rpm (11,1 %). Due to the use of internal capacitive compensation, the power factor of the modified SEMC increases to 0,71 (by 20,3 %), and the electrical efficiency, which takes into account only the mechanical useful power for transporting the raw material, increases from 9,58 to 11,4 %. It should be noted that due to the increase in losses in the steel of the modified SEMC, the amount of heat that will be directed to the processed material will increase, therefore the thermal efficiency of the modified SEMC will also increase.

Experimental studies of the mock-up sample of SEMC. To verify the simulation results, a mock-up sample of the basic (without internal capacitive compensation) variant of the two-stator SEMC was tested. Nominal data of SEMC: power consumption P = 2078 W; supply voltage U = 80 V; current consumption I = 30 A; power factor cosφ = 0,5; the number of poles is 6; rotation frequency with coordinated rotation of the magnetic fields of individual modules n = 450 rpm. Figure 12 shows the nodes of the SEMC mock-up sample with the determination of the measurement zones of electromagnetic and temperature parameters.

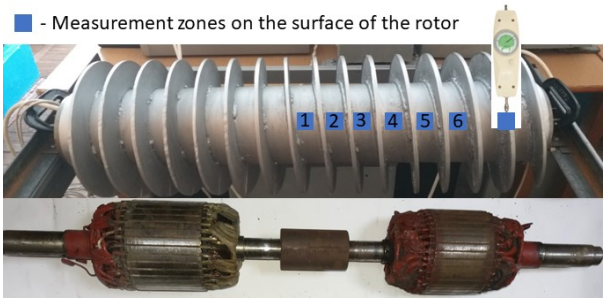

Fig. 12. Distribution of electromagnetic, temperature and mechanical parameters measurement zones on the surface outer rotor of the SEMC mock-up sample

Figure 12 shows the corresponding location of the system of adjacent stators, which are placed in the cavity of the external rotor, as well as the location of the dynamometer for measuring the starting torque.

Electromagnetic and temperature parameters were measured on mock-up samples in the short-circuit mode (braked rotor) when the supply voltage was reduced to the level at which the rated current was reached.

The following measuring devices were used during the research: Tenmars TM-191 Magnetic Field Meter, designed for measuring ultra-low frequency electromagnetic fields from 30 Hz to 300 Hz; Tenmars TM-190 Multi Field EMF Meter – a device for measuring high-frequency electromagnetic fields in the frequency range from 50 MHz to 3,5 GHz and low-frequency electric and magnetic fields in the frequency range of 50-60 Hz; infrared, optical pyrometer Benetech GM533A, measuring range –50 ... +530 °C, imaging index 12:1, coefficient of thermal radiation 0,1–1, spectrum 5–14 μm; thermal imager Xintest HTI HT-18, thermal sensitivity 0,07 °C, temperature range: –20...+300 °C, image capture frequency 8 Hz, wavelength range 8-14 μm; analog spring universal dynamometer NK-300, used to measure the starting torque, accuracy class 0,5 %; K540-3 transformer parameters meter was used to measure the electrical parameters of the SEMC. Table 2 presents the experimental data of electrical and energy parameters of the mock-up sample of the basic (without internal capacitive compensation) version of the two-stator SEMC.

The SEMC load was carried out by the frictional effect of the mechanical brake on the end part of the rotor-screw. The load torque is 7,4 N·m. Power, current and voltage were measured by K540-3 transformer parameters meter.

Table 3 presents the experimental data of the surface electromagnetic parameters of the mock-up sample of the basic (without internal capacitive compensation) version of the two-stator SEMC. Magnetic flux density, electric field strength, electromagnetic radiation flux density were measured in the short-circuit mode at the minimum possible distance of 1 mm from the surface of the SEMC rotor.

Table 2

Experimental data of electrical and energy parameters of the mock-up sample of SEMC

Voltage, V	Power, W		Current in the short-circuit mode, A		Current at load, A		Starting torque of the module, N·m	Power factor		Slip
	load mode	short-circuit mode	total	of the module	total	of the module		load mode	short-circuit mode	
60,5	1120	1320	23,17	11,6	23	11,5	4	0,508	0,546	0,84
70	1594	1876	27,5	13,75	26,2	13,1	5,6	0,5	0,556	0,73
77	1878	2266	30,12	15,7	28,5	14,3	12,3	0,492	0,562	0,63
81	2040	2384	33,7	22,5	29,8	14,9	13,7	0,486	0,57	0,55

Table 3

Experimental data of surface electromagnetic parameters of the SEMC mock-up sample

Measurement zones	Parameters at supply voltage $U = 81$ V				
	Magnetic flux density, mT	Electric field strength, V/m	Electromagnetic radiation flux density, mW/m²	Temperature, °C	
				Fig. 16,*a*	Fig. 16,*b*
1	60	0,03	0,7	28,5	48
2	100	0,03	0,9	30,5	51
3	170	0,03	1,8	41,2	62
4	400	0,2	523	61	74
5	380	0,15	520	63,3	76,2
6	410	0,15	525	63,1	76,3

Figure 13 shows a diagram of a measuring bench for recording current oscillograms using ACS758 current sensors on the Hall effect with a sensitivity of 40 mV/A.

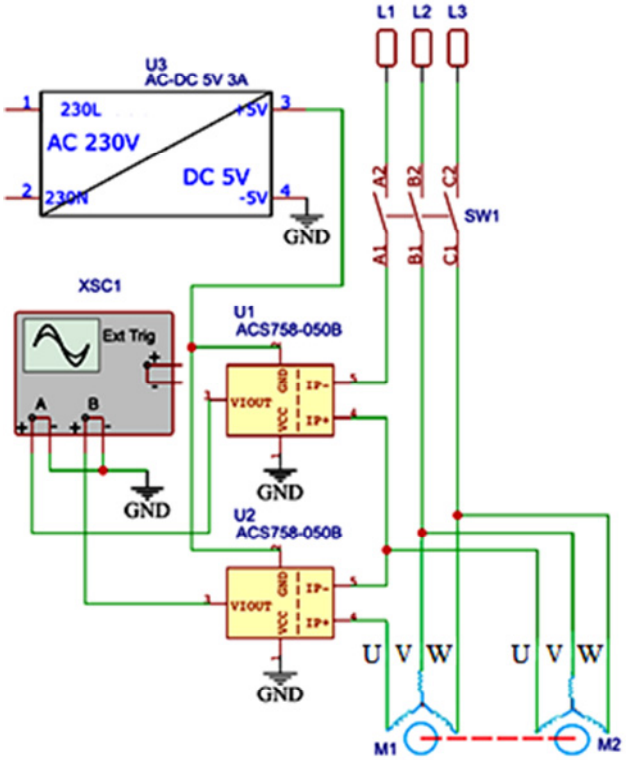

Fig. 13. Diagram of the measuring bench

Figure 14 shows the oscillograms of the total current of the SEMC and the current of a separate module at a supply voltage of $U = 81$ V.

Fig. 14. Oscillograms of total current 1 and the current of a separate module 2 of SEMC: start-up period (*a*), after 7 minutes of SEMC operation (*b*)

Due to the change in the parameters of the stators and the rotor, there is a decrease in the amplitudes and effective

values of the currents by up to 5 % during 7 minutes of operation of the SEMC. A comparison of the distribution of the temperature field on the surface of the rotor of the SEMC mock-up sample with the simulation results was made. Thermograms were recorded after 7 minutes of operation in the short-circuit mode at a voltage $U = 73$ V. In Fig. 15,*a* the mock-up sample with an arbitrary azimuthal location of the frontal parts of adjacent stators is shown.

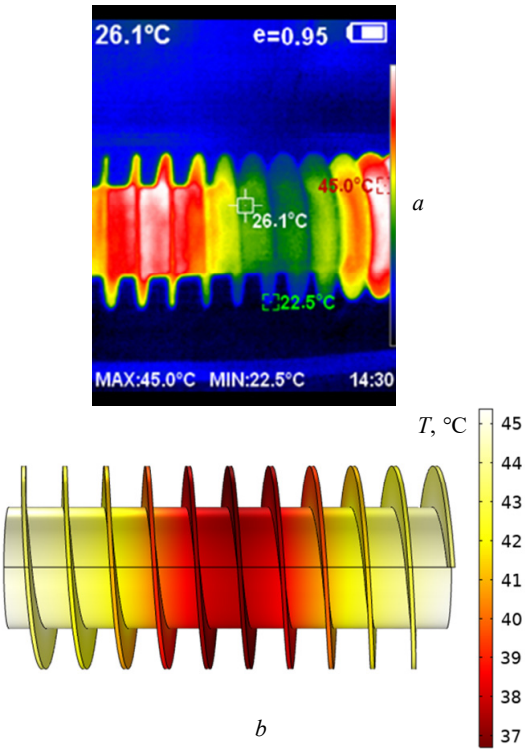

Fig. 15. Temperature distribution on the surface of the SEMC rotor: experimental thermogram of the mock-up sample after 7 minutes of rotation at idle speed at a voltage of 81 V, rotation frequency 450 rpm (*a*), simulation result (*b*)

The results of experimental studies (Tables 2, 3, Fig. 14, 15), namely of parameters and characteristics of the SEMC module: starting torque and current; torque and current under load, magnetic flux density, rotor surface temperature with an accuracy of 11 % coincide with the calculated ones, which indicates the reliability of the SEMC mathematical model.

Conclusions.

1. A method of spatial shift of the main and additional stator windings and internal capacitive compensation is proposed and a comparative analysis of the connection schemes and spatial arrangement of the stator windings of the basic and modified versions of the screw electromechanical converter (SEMC) is performed.

2. It has been proven that the application of internal capacitive compensation over a wide range of changes in the angle of spatial shift of the main and additional windings and compensating capacitors allows changing the value and phase of currents, magnetomotive forces and other electrical quantities. A significant (by 29 %) increase in the electromagnetic torque and a decrease in its extreme pulsations have been achieved for the modified SEMC.

3. Due to the use of internal capacitive compensation, an increase in energy performance is achieved: the power factor of the modified SEMC increases by 20,3 %, and the electrical efficiency, which takes into account only the mechanical useful power for transporting raw material, increases by 1,86 %.

4. The use of the proposed method of spatial shift of the main and additional stator windings and internal capacitive compensation is promising for increasing the energy performance of SEMC.

Acknowledgment. The work was carried out with the support of the Ministry of Education and Science of Ukraine (projects DB No. 0120U102105 and No. 0121U113746).

Conflict of interest. The authors declare no conflict of interest.

REFERENCES

1. Zhitao Han, Li Ding, Gang Wang. Experimental Investigation of Induction Motor Power Factor and Efficiency Impacted by Pulse Width Modulation Power and Voltage Controls of Variable-Frequency Drives. *ASHRAE Transactions*, 2021, vol. 127, pp. 817-828.

2. Bortoni E.C., Bernardes J.V., da Silva P.V.V., Faria V.A.D., Vieira P.A.V. Evaluation of manufacturers strategies to obtain high-efficient induction motors. *Sustainable Energy Technologies and Assessments*, 2019, vol. 31, pp. 221-227. doi: https://doi.org/10.1016/j.seta.2018.12.022.

3. Mbinkar E.N., Asoh D.A., Kujabi S. Microcontroller Control of Reactive Power Compensation for Growing Industrial Loads. *Energy and Power Engineering*, 2022, vol. 14, no. 9, pp. 460-476. doi: https://doi.org/10.4236/epe.2022.149024.

4. Habyarimana M., Dorrell D.G., Musumpuka R. Reduction of Starting Current in Large Induction Motors. *Energies*, 2022, vol. 15, no. 10, art. no. 3848. doi: https://doi.org/10.3390/en15103848.

5. Antar R.K., Suliman M.Y., Saleh A.A. Harmonics resonance elimination technique using active static compensation circuit. *Bulletin of Electrical Engineering and Informatics*, 2021, vol. 10, no. 5, pp. 2405-2413. doi: https://doi.org/10.11591/eei.v10i5.3148.

6. Ferreira F.J.T.E., de Almeida A.T. Novel Multiflux Level, Three-Phase, Squirrel-Cage Induction Motor for Efficiency and Power Factor Maximization. *IEEE Transactions on Energy Conversion*, 2008, vol. 23, no. 1, pp. 101-109. doi: https://doi.org/10.1109/TEC.2007.914355.

7. Guo J., Ma X., Ahmadpour A. Electrical–mechanical evaluation of the multi–cascaded induction motors under different conditions. *Energy*, 2021, vol. 229, art. no. 120664. doi: https://doi.org/10.1016/j.energy.2021.120664.

8. Jagiela M., Garbiec T. Determination of best rotor length in solid-rotor induction motor with axial slitting. *Archives of Electrical Engineering*, 2012, vol. 61, no. 2, pp. 267-276. doi: https://doi.org/10.2478/v10171-012-0022-2.

9. Zablodskiy M., Gritsyuk V., Rudnev Y., Brozhko R. Three-dimensional electromagnetic field model of an auger electromechanical converter with an external solid rotor. *Mining of Mineral Deposits*, 2019, vol. 13, no. 4, pp. 99-106. doi: https://doi.org/10.33271/mining13.04.099.

10. Milykh V.I. Numerical-field analysis of active and reactive winding parameters and mechanical characteristics of a squirrel-cage induction motor. *Electrical Engineering & Electromechanics*, 2023, no. 4, pp. 3-13. doi: https://doi.org/10.20998/2074-272X.2023.4.01.

11. Trisha, Gupta G.S., Shiva Kumar S. Review of the Parameter Estimation and Transient Analysis of Three-Phase Induction Motor. *Lecture Notes in Electrical Engineering*, 2021, vol. 693, pp. 223-232. doi: https://doi.org/10.1007/978-981-15-7675-1_21.

12. Nasir B.A. An Accurate Iron Core Loss Model in Equivalent Circuit of Induction Machines. *Journal of Energy*, 2020, vol. 2020, pp. 1-10. doi: https://doi.org/10.1155/2020/7613737.

13. Ekpo E.G., Umoh G.D., Udokah Y.O.N. Effect of Phase-Shift in Six-Phase Induction Machine. *Journal of Emerging Trends in Engineering and Applied Sciences*, 2022, vol. 13, no. 6, pp. 215-226.
14. Saneie H., Nasiri-Gheidari Z. Performance Analysis of Outer-Rotor Single-Phase Induction Motor Based on Magnetic Equivalent Circuit. *IEEE Transactions on Industrial Electronics*, 2021, vol. 68, no. 2, pp. 1046-1054. doi: https://doi.org/10.1109/TIE.2020.2969125.
15. Sharma U., Singh B. Robust design methodology for single phase induction motor ceiling fan. *IET Electric Power Applications*, 2020, vol. 14, no. 10, pp. 1846-1855. doi: https://doi.org/10.1049/iet-epa.2020.0017.
16. Rezazadeh G., Tahami F., Capolino G.-A., Nasiri-Gheidari Z., Henao H., Sahebazamani M. Improved Design of an Outer Rotor Six-Phase Induction Motor With Variable Turn Pseudo-Concentrated Windings. *IEEE Transactions on Energy Conversion*, 2022, vol. 37, no. 2, pp. 1020-1029. doi: https://doi.org/10.1109/TEC.2021.3126538.
17. Tornello L.D., Foti S., Cacciato M., Testa A., Scelba G., De Caro S., Scarcella G., Rizzo S.A. Performance Improvement of Grid-Connected Induction Motors through an Auxiliary Winding Set. *Energies*, 2021, vol. 14, no. 8, art. no. 2178. doi: https://doi.org/10.3390/en14082178.
18. Di C., Petrov I., Pyrhonen J.J. Design of a High-Speed Solid-Rotor Induction Machine With an Asymmetric Winding and Suppression of the Current Unbalance by Special Coil Arrangements. *IEEE Access*, 2019, vol. 7, pp. 83175-83186. doi: https://doi.org/10.1109/ACCESS.2019.2925131.
19. Zablodsky N., Chuenko R., Gritsyuk V., Kovalchuk S., Romanenko O. The Numerical Analysis of Electromechanical Characteristics of Twin-Screw Electromechanical Hydrolyzer. *2021 11th International Conference on Advanced Computer Information Technologies (ACIT)*, 2021, pp. 130-135. doi: https://doi.org/10.1109/ACIT52158.2021.9548392.
20. Kaplun V., Makarevych S., Chuenko R. Modelling of Asynchronous Motor with Split Stator Windings on the Principle of a Rotary Autotransformer. *Przeglad Elektrotechniczny*, 2022, vol. 98, no. 3, pp. 39-43. doi: https://doi.org/10.15199/48.2022.03.10.
21. *AC/DC Module User's Guide*. COMSOL Inc., Burlington, MA, USA, 2018.
22. Rezazadeh G., Tahami F., Capolino G.-A., Vaschetto S., Nasiri-Gheidari Z., Henao H. Improvement of Concentrated Winding Layouts for Six-Phase Squirrel Cage Induction Motors. *IEEE Transactions on Energy Conversion*, 2020, vol. 35, no. 4, pp. 1727-1735. doi: https://doi.org/10.1109/TEC.2020.2995433.
23. *Heat Transfer Module User's Guide*. COMSOL Inc., Burlington, MA, USA, 2018.

Received 16.10.2023
Accepted 12.01.2024
Published 01.05.2024

M.M. Zablodskiy[1]*, Doctor of Technical Science*, *Professor*,
R.M. Chuenko[1]*, PhD*, *Assistant Professor*,
S.I. Kovalchuk[1]*, PhD, Junior Research Scientist,*
H.V. Kruhliak[1]*, Assistant,*
O.I. Kovalchuk[1]*, Postgraduate Student,*
[1] National University of Life and Environmental Sciences of Ukraine,
12, Heroyiv Oborony Str., Kyiv, 03041, Ukraine,
e-mail: stas_kovalchuk@outlook.com (Corresponding Author)

How to cite this article:
Zablodskiy M.M., Chuenko R.M., Kovalchuk S.I., Kruhliak H.V., Kovalchuk O.I. Internal capacitive compensation of the reactive power of the screw electromechanical converter. *Electrical Engineering & Electromechanics*, 2024, no. 3, pp. 11-21. doi: https://doi.org/10.20998/2074-272X.2024.3.02